MANSOURA JOURNAL OF PHYSICS
Official Journal of Faculty of Science, Mansoura University, Egypt
E-mail: scimag@mans.edu.eg ISSN: 2974-4954

Characterization and antibacterial activities of different silver-doped hydroxyapatite compositions

S. Mohamed*, H. Doweidar, H. Kamal, M.I. Abdelghany

Glass Research Group, Physics Department, Faculty of Science, Mansoura University, Mansoura 35516, Egypt

**Corresponding author: sara.mohamed@students.mans.edu.eg (S. Mohamed), ph_abdelghany@yahoo.com (M.I. Abdelghany).*

Received:6/6/2021
Accepted: 27/6/2021

Abstract: Silver-doped calcium phosphate was synthesized using the solution route. Hydroxyapatite (HA), beta tri-calcium phosphate (β-TCP) and Ag-components were demonstrated in the X-ray diffraction (XRD) patterns and Fourier transform infrared spectroscopy spectra (FTIR). Infection can threaten the long-term success of a biomaterial utilized in surgery. The antibacterial effects toward *Staphylococcus aureus (S. aureus)* was determined by agar disk-diffusion technique and determination of the minimal inhibitory and maximum bactericidal silver concentrations. Comparing with HA, Ag-HA exhibited an antibacterial effect on *S. aureus* to be 0 mm for HA, and in range (2-12) mm with Ag addition. XRD peaks are broad at low temperatures, indicating that the crystallinity of silver-hydroxyapatite (Ag-HA) is grown by increasing thermal treatment at low silver concentration. High Ag-content increased the crystallinity of the obtained phases to be in range of (64-73) % for 700 °C/8h, and (51-73) % for 900 °C/8h.

keywords: Hydroxyapatite; Antibacterial; Antibiotics; *S.* aureus pathogen

1. Introduction

Considerable attention is paid to synthetic grafts, including hydroxyapatite (HA), tri-calcium phosphate (TCP), bioactive glass, and glass ceramics [1]. Graft material that can resorb is often desirable, making space for new bone formation, but the poor resorbability of stoichiometric HA causes a limiting factor [2]. Nevertheless, the bone conductive effect is limited since bone growth can occur in porous and dense HA [3].

Like HA, β-TCP and Biphasic calcium phosphate (BCP), synthetic calcium phosphates have been used as bone implants [4]. These orthopedic implants demonstrate strong compatibility and new bone development on implants without fibrous encapsulation [5]. Well-crystallized and sintered HA, however, usually showed limited in-vivo resorption that delayed new bone formation rates [6]. As explained by Kilian et al. [7] suggested that osteoclasts and macrophages may phagocytize and dissolve disposed HA, whereas sintered ceramics are nondegradable and remain for years at the place of implantation after surgery.

HA is formed by Ca^{+2}, PO_4^{-3}, and OH^- ions, and these ions are in the proper orientation configuration and in sufficient numbers to form the stable crystal of apatite [8] . The presence of many foreign ions is characterized by synthetic biological apatite, which plays a significant metabolic role [8]. In addition, HA has the potential to strengthen therapeutic bone formation by anionic substitution (carbonate, fluoride, and silicate) and/or cationic substitution (magnesium, strontium, zinc, iron, and silver) [8]. Apatite substituted with the relevant ions is also considered to be an attractive biomaterial for hard tissue replacement/repair [9].

The adhesion of HA to the Ti substrate is significant for the implant to function suitably in physiological conditions. International standards demand that the BS value be at least 15 MPa [10]. The BS measured for the Mn-HA film was 13.9 ± 3.7 MPa, nearly two times

higher than 6.7 ± 2.1 MPa for pure HA film, which provided predominantly high BS to meet the requirements of international standards [10]. This BS value of the Mn-HA film was higher than that of the HA film prepared by a traditional electrophoretic deposition process (11 MPa) [11].

While HA is the main component of natural hard tissues in the mineral process, the problem still exists in pure HA nanoparticle synthesis [12]. HA has been categorized as it owns several limitations. This is the absence of antimicrobial activity that raises the risk of microbial colonization and adherence to HA-implanted microorganisms or HA-coated biomaterials [12]. Implant infections can lead to prolonged, terrible pain, leading to implant failure and removal from their location [12].

Silver (Ag) is of particular interest in this respect, as its inhibitory impact on many pathogenic bacteria and microorganisms has long been recognized [13]. It has been established for centuries that silver ions show significant inhibitory effects against several bacterial strains [14]. Ag has been introduced into many biomaterials, including Ca-P such as HA and TCP, in its many oxidation states (Ag^0, Ag^{+1}, Ag^{+2}, and Ag^{+3}) [14].

In order to minimize the length of treatment by having a localized antibacterial effect, the implants should have antibacterial properties, thus reducing the need and side effects of systemic therapies, thus enhancing their efficacy [15]. An inorganic antibacterial agent, Silver is historically known for its wide-spectrum antimicrobial activities against bacteria, viruses, algae, and fungi [15].

Gram-positive bacteria such as (*S. aureus)*, *Staphylococcus epidermidis*, and *Streptococcus spp.* are broadly responsible for these infections. *S. aureus* is a significant problem for surgery-related facilities infections [16].

Recently, nanocrystalline silver has shown excellent antimicrobial activity compared to other available silver antimicrobial agents such as silver nitrate or silver sulfadiazine, not only due to the rapid release of silver cation (Ag^+), but also due to the release of other silver species such as Ag^0 as well [17 Yin HQ, Langford R, Burrel RE. Comparative evaluation of the antimicrobial activity of ACTI Coat antimicrobial barrier dressing. J Burn Care Rehabil 1999; 20:195–200].

This study aims to characterize the synthesized silver-hydroxyapatite compositions, in addition, to investigate the physical and antibacterial properties of prepared compositions to be recommended for bio-applications.

2. Experimental techniques

Five compositions of the formula $\left[Ca_{10-x}Ag_x\left(PO_4\right)_6\left(OH\right)_2\right]$ were prepared with different silver contents of x = 0.0, 0.4, 0.8, 1.2, and 1.6 mole with constant (Ca+Ag)/ P to equal 10:6. The used raw materials are $Ca(NO_3)_2.4H_2O$, $(NH_4)_2HPO_4$ and $AgNO_3$ as precursors.

In the solution approach, ethanol and distilled water were utilized as solvent that generated a relatively viscous solution as a result. The inclusion of ethanol in $Ca(NO_3)_2$-$4H_2O$ and $(NH_4)_2HPO_4$ solutions was found to support the transitions during production of calcium phosphates, from the cluster to crystallite forms. Ethanol creates thermally stable hydroxyapatite at a lower temperature than other methods [10].

With the addition of Ca-containing or (Ag+Ca)-containing solution into the P-containing solution, a steady increase in viscosity is noticed throughout the creation of a solution with pH=9, where pH was controlled by (NH_4OH). Depending on the value of x, the resultant solution has white, yellow, or grey colors following the ageing process. To complete the reaction between Ca and P molecular precursors, ageing time (72h) was desired [11,12].

X-ray diffraction (XRD) was used to determine the phases of the dried and heat-treated (H.T.) compositions using a Bruker Axs-D8 Advance diffractometer with a CuK_α source (= 0.15406 nm). Data was collected in step mode with 0.02 second intervals over a 2°–70° range with a dwell period of 0.4 seconds. X'Pert High Score Plus was used to determine the phases (PANalytical, Netherlands).

Using the KBr disc technique, FTIR spectra of all examined compositions were acquired at room temperature. The investigated substances were ground to a fine powder and blended

1:100 in weight with KBr. The spectra were obtained using a mattson 5000 FTIR spectrometer with a resolution of 2 cm1 in the wavenumber range of 400 to 2000 cm^{-1}. Each sample's spectrum is the average of 30 scans.

The antibacterial sensitivities of HA and Ag-HA were evaluated against the bacterial species *S. aureus* using the agar disk-diffusion technique. For disk diffusion (commonly known as the Kirby–Bauer disc diffusion method or antibiotic sensitivity test), solidified nutrient agar medium plates were prepared and bacterial cultures were swabbed on these plates. The bacterial colonies formation was examined and photographed.

3. Results and discussion

3.1.XRD characterization

Figure 1 and Figure 2 show XRD patterns of ($Ca_{10-x}Ag_x(PO_4)_6(OH)_2$) compositions, where; ($x$ = 0, 0.4, 0.8, 1.2 and 1.6 mole). The patterns include those of as-prepared samples (Fig. 1) and heat-treated samples. The thermal treatment takes place as a function of temperature and time at (700 ℃ and 900 ℃) for 8 hours. There are obvious changes in the patterns due to the change in temperature and silver content. Depending on the phase identification, the different phases are identified as: HA phase [JCPDS File No. 76-0694], β-TCP phase [JCPDS File No. 09-0169], metallic Ag phase [JCPDS File No. 01-1167], Ag_3O_4 phase [JCPDS File No. 40-1054] and Ag_3PO_4 [JCPDS File No. 70-0702].

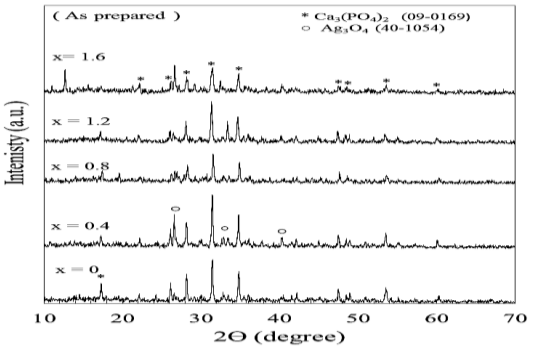

Figure 1. XRD patterns of as-prepared $Ca_{10-x}Ag_x(PO_4)_6(OH)_2$ compositions.

XRD patterns of as-prepared Ag-HA compositions are displayed in Fig.1, which are related to crystalline β-TCP phase in the sample having x=0. Upon Ag substitution, the obtained phases are TCP and silver - related phase (Ag_3O_4). The characteristic peaks of the latter appear at 2Θ ~ 26°, 34° and 41°.

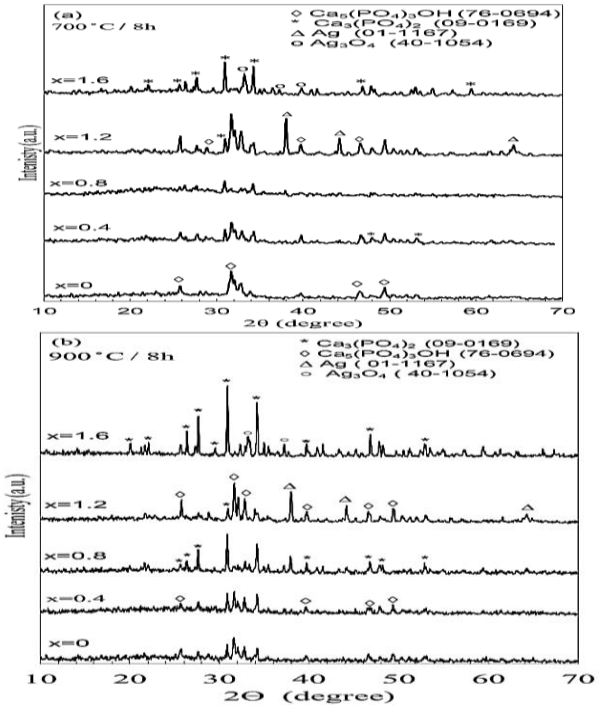

Figure 2. XRD patterns of $Ca_{10-x}Ag(PO_4)_6(OH)_2$ compositions; H.T. for 8h, 700 °C (a) and 900 °C (b).

The first step of H.T. was applied at 700 °C (8h) on an undoped sample, its XRD pattern (Fig. 2-a) shows that the crystalline phase is presented as HA. Further silver substitution 0.4 Ag-HA, Ag contributed to form TCP phase at 2Θ ~ 31°. 0.8 Ag-HA is glass-ceramic TCP phase. At high Ag concentration 1.2 Ag-HA, (HA+TCP) phases are observed besides of metallic Ag at 2Θ ~ 38°. At 1.6 Ag-HA, TCP is the dominant phase with Ag_3O_4. Metallic Ag phase can be observed at 2Θ ~ 38° and 45°. Additions of silver content activate formation of (HA+TCP) phases. Owing to these results, the role of Ag may be considered as a nucleating agent, as reported before [13,14]. The crystalline phases present in figure 2-b can be listed in Table I.

Table I: Crystalline phases in different prepared compositions

Sample (900 °C/8h)	Crystalline phases
0 Ag-HA	HA+β-TCP
0.4 Ag-HA	HA+β-TCP
0.8 Ag-HA	β-TCP+Ag
1.2 Ag-HA	HA+β-TCP+Ag
1.6 Ag-HA	β-TCP+Ag_3O_4

β-TCP, as phases for bio-applications, have been successfully synthesized using the solution method. The metallic silver and Ag phases obtained from XRD patterns seem to activate formation of Ag-HA compositions. From XRD patterns, it appears that H.T. is a necessary condition to form HA and/or β-TCP phases. silver doping with different concentrations tends to form HA, TCP, (HA+TCP) and other phases that belong to silver ion.

Recently, a lot of research on the characteristics of HA has been studied, but some basic principles of HA are still not very clear. Many studies agree that HA is stable in water vapor atmosphere up to 1200 °C [15], while some others argued that HA may be partly decomposes (in the temperature range 800-1200 °C) into beta-tricalcium phosphate [16-18].

During the thermal treatment, behavior of CaP is affected by various factors, like, atmosphere of sintering, ratio of Ca/P, method and conditions of powder synthesis, type and amount of impurities, sample size, particle size, etc. [26].

During thermal treating HA undergoes the following processes:

- dehydration (separation of adsorbed water);
- dehydroxylation (separation of structured water), forming oxy-hydroxyapatite (OHA) and oxyapatite (OA); • HA decomposition with formation of other phases as β-TCP [26].

Raynaud et al. [27] also found partial decomposition of HA into tricalcium phosphate. When the HA was H.T. at 900 and 1000 °C and/or with Ag doping at lower temperatures of 700 and 800 °C, this decomposition into tricalcium phosphate was observed in the current work.

Hudon and Jung [28] presented recently a very thorough study on the phase stability of calcium phosphates and came to the conclusion that the β-α and the α-α‟ phase transitions occur at 1125 °C and 1470 °C, respectively. They also pointed out that these temperatures vary over a very broad range in the presence of elemental impurities. Enderle et. al [29] reported for example that the β-α phase transition temperature increased from 1150 °C with 0 mol% Mg phosphate to 1540 °C with 8 mol% Mg phosphate. It is generally deduced that there is an increase in crystallinity with increasing silver concentration.

3.2. FTIR spectra:

FTIR spectra of the as-prepared and heat-treated compositions without and with different contents of silver at different temperatures (700 and 900 °C) for (8h) are presented in Fig.2.1 and Fig.2.2. In all reported FTIR spectra of the studied samples, there are two basic absorption envelopes in the region 900-1200 cm^{-1} and 500-700 cm^{-1} which split into two or three distinct peaks. In addition, other absorption bands appear in some cases at 420-450 cm^{-1}, 820 and 1380 cm^{-1}, 715 cm^{-1} and 960, 975 and 1100 cm^{-1}. The different bands and their assignments are listed in Table II.

Table II: List of FTIR absorption bands and their assignments of the studied samples.

Wavenumber (cm^{-1})	Assignments	References
960, 975 and 1100	β-TCP shoulders	[30]
715	$P_2O_7^{4-}$	[30]
500-603	PO_4^{3-} bending mode	[30]
630	OH^- liberationalmode	[31]
820 and 1380	NO_3^- or CO_3^{2-}	[27,31,32]
1032 and 1094	PO_4^{3-} stretching mode	[30]

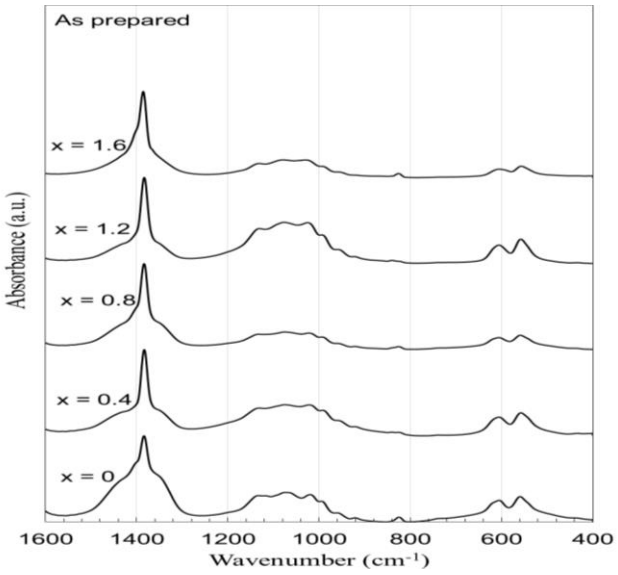

Figure 3. Normalized FTIR spectra of $Ca_{10-x}Ag_x(PO_4)_6(OH)_2$ compositions

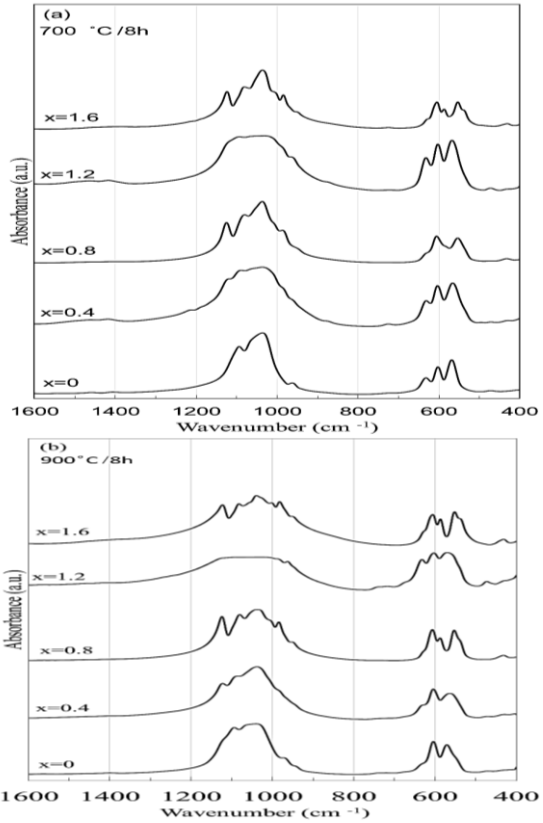

Figure 4 Normalized IR spectra for Ca10−xAg $(PO4)_6(OH)_2$ where) ؛x=0, 0.4, 0.8, 1.2 and 1.6) compositions; H.T. for 8h, 700 °C (a) and 900 °C (b).

Figure 3 of as prepared samples presents the peak at approximately 1380 cm^{-1} and ~ 817 cm^{-1} that is related to NO^{-3}. The region between 900-1200 cm^{-1} and the duplet bands at 500-700 cm^{-1} have small area under the bands which increases as H.T. process takes place as seen in Figure 4 (a, b).

The FTIR spectra of the calcium phosphate precipitates treated at different temperatures (700 °C and 900 °C) for 8h time intervals are significantly altered as the Ag-HA crystals combined with TCP mature.

Figure 4-a presents the thermal treatment of 700 °C for 8h. For *x*=0, the region (900-1200) cm^{-1} have two shoulders (1100 and 960) cm^{-1} at with the same previously discussed assignments. The clearly resolved υ_3 band and the narrow spectral region of υ_3 and υ_4 are related to the well crystallized HA [19]. In addition, OH^- at 630 cm^{-1} shows the HA formation and also appears at *x*=0.4 and 1.2. The spectral region of υ_1 and υ_3 is broad and υ_4 is with high intensity which reflects the semi crystallized HA [27]. The absence of OH^- band and the splitting of a shoulder at 1100 cm^{-1} of β-TCP denote the formation of well crystallized TCP as presented for *x*=1.6 and poor crystallized TCP for *x*=0.8. These results match with XRD patterns.

Figure 4-b shows 900 °C/8h, *x*=0, *x*=0.4 and *x*=1.2 refer to well crystallized HA. *X*=0.8 and 1.6 are well crystallized TCP. It was discovered that the type of apatite generated, whether weakly or well-crystallized, may be determined. The well-crystallized apatite's 900-1200 cm^{-1} spectral contour is significantly narrower, and the υ_1 at (950-970) cm^{-1} component is clearly resolved [22]. Pleshko et al. [33] presented a unique IR approach for testing HA material crystallinity based on variations in the phosphate υ_1 and υ_3 absorbance spectrum area between 900 and 1200 cm^{-1}. Termine and Posner (1966) developed an IR technique based on phosphate υ_4 mode alterations to measure the percentage of apatite crystallinity materials [34].

FTIR data demonstrate the existence of OH^- at the triplet peak 630 cm^{-1}, which corresponds to the production of HA or (HA+TCP), and its absence suggests the presence of TCP at (960 cm^{-1} and 1100 cm^{-1}) [30].

Silver doping at various concentrations has no effect on the acquired functional groups, but it does play a role in controlling HA partial decomposition into TCP, HA growth from TCP, and the degree of crystallinity of HA and/or TCP, in addition to heat treatment and time interval.

Shirkhanzadeh at al. [35] stated that no extra peaks were observed in the FTIR spectrum between the wavelengths of 400 and 4000 cm^{-1} when HA was doped with Ag. Nath et al. stated that the Ag-O band of Ag_2O and AgO phases could not be detected by the 400 – 4000 cm^{-1} wavelength. FTIR results did not show the presence of silver ions. FTIR spectrum of the compound Ag-HA was not observed. It is thought that the reason for this is that as explained as, the silver substitutions in the HA take place in accordance with the formula $Ca_{10-x}Ag_x(PO_4)_6(OH)_2$ [36].

3.3. Antibacterial Assessment

The antimicrobial activities of the Ag–HA compositions were assessed by zone plate clearance/inhibition (ZOC/ZOI) This represents respective gram-positive bacteria commonly found on the skin, in chronic wounds and in orthopedic implant sites.

In the zone assay method, antimicrobial efficacy is proportional to the size of the colony-free zone surrounding the tablet, where bacterial growth was inhibited.

Figure 5 shows the antibacterial effects of silver addition within HA against *S. aureus* pathogen using agar disk-diffusion technique. The average inhibition zones are listed in Table III.

Table III: The average inhibition zones of the Ag-HA tablets Degree.

	Sample	**Inhibition Zone (mm)**
As-prepared	0	0
	0.4	5
	0.8	7
	1.2	8
	1.6	12
H.T Degree	**Sample**	**Inhibition Zone (mm)**
700 °C/8h	0	0
	0.4	4
	0.8	5
	1.2	5
	1.6	6

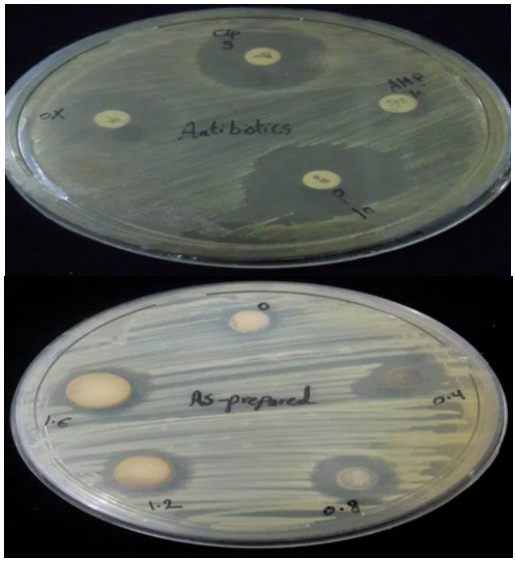

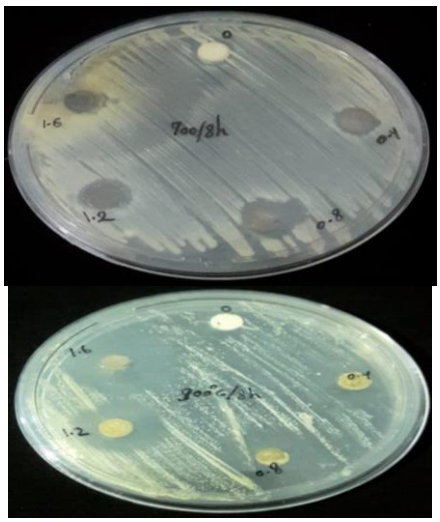

Figure 5. The antibacterial effects of silver addition within HA and different antibiotics against *S. aureus* pathogen using agar disk-diffusion technique.

No antibacterial activity is detected for the 0 Ag-HA compositions. The inhibition of bacterial growth around the tablets might be due to the release of silver ions from HA, β-TCP or (HA+ β-TCP) lattices into the surrounding medium. These values increase with increasing amount of Ag content into Ca-P matrices.

Two mechanisms have been developed to explain the antimicrobial effects of Ag-HA:

- First, that microorganisms adhere to the surface by electrostatic force and interact directly with metal ions [37,38].
- The second mechanism is that the slow release of Ag from HA and/or TCP can inhibit bactericidal activity in the medium [39].

Silver ions have a variety of ways for interfering with cell growth. In addition, silver has the ability to produce novel antimicrobial agents, drug delivery formulations, coatings of biomaterials, products for regeneration and improved therapeutics (*Zafar et al*., 2019). The release of Ag^{+} ions from Ag nanoparticles (AgNPs) to interfere with membrane permeability, or microbial killing by direct contact with bacteria, are two mechanisms for silver's antibacterial action (*Fu et al*., 2016).

It can be seen that the migration of the Ag^{+} ions to the organic medium after 48 h of incubation occurs differently, depending on the bacterial strain and the film composition.

Different antibiotics (Oxacillin, Ampicillin, Picillin, Ciprofloxacin) are used as a reference

besides of Ag-Ca-P matrices to compare between their antibacterial sensitivity.

The noticed results show that, the size of the colony-free zone surrounding the antibiotic tablets are larger than those of Ag-Ca-P biomaterials and their effects begin after 12 hours, although of that, Ag-Ca-P compositions show results after 24 hours. These results according to the previous explanations can be discussed as, the antibiotics have high release so they have the tendency to kill the pathogen in short interval but, from previous publications, antibiotics show disadvantages of:

- By body flood, antibiotics loaded into implant material appear to be easily flushed out, resulting in long-term post-surgical infections.
- Bacteria have the ability to resist the effect of antibiotics.

4. Conclusion

Calcium phosphate nanoparticles as, HA, TCP and HA+TCP (BCP) can be doped with silver, resulting in a bactericidal effect against *S. aureus* with silver concentrations of 0.4-1.6 mole**.** The lethal silver concentrations against bacteria, i.e. *S. aureus*, begin with a minimum concentration at x=0.4. Such silver-doped calcium phosphate nanoparticles could be employed to generate a local antibacterial effect, but care must be taken not to expose the surrounding tissue to cytotoxic silver concentrations. antibacterial properties of silver additions within HA against the *S. aureus* pathogen were investigated. The average clearance zones are in range between (2-12 mm). The phosphate and hydroxyl vibrations in the FTIR results also reveal the typical characteristics of apatite and β-TCP.

4. References

1. Schepers E.J., P. Ducheyne, L. Barbier and S, Schepers, (1993). Bioactive glass particles of narrow size range: a new material for the repair of bone defects. *Implant dentistry*, **2(3)**, pp.151-157.
2. Schepers E., M.D. Clercq, M.D. Ducheyne, and R. Kempeneers, (1991). Bioactive glass particulate material as a filler for bone lesions. *Journal of oral rehabilitation*, **18(5),** pp.439-452.
3. Schepers E., M.D. Clercq, P. Ducheyne and R. Kempeneers, (1991). Bioactive glass particulate material as a filler for bone lesions. *Journal of oral rehabilitation*, **18(5),** pp.439-452.
4. Elliott J.C., (1994). Structure and chemistry of the appetites and other calcium orthophosphates, *Hydroxyapatite and nonstoichiometric appetites*. **18**, pp.111-189.
5. Spector M., (1994). Inorganic bovine bone and ceramic analogs of bone mineral as implants to facilitate bone regeneration. *Clinics in Plastic Surgery*, **21(3),** pp.437-444.
6. Hing K.A., S.M. Best, K.E. Tanner, W. Bonfield and P.A. Revell, (2004). Mediation of bone ingrowth in porous hydroxyapatite bone graft substitutes. Journal of Biomedical Materials Research Part A: *An Official Journal of The Society for Biomaterials, The Japanese Society for Biomaterials, and The Australian Society for Biomaterials and the Korean Society for Biomaterials*, **68(1),** pp.187-200.
7. Kilian O., S. Wenisch, C. Heiss, U. Horas, E. Dingeldein, and R. Schnettler, (2002). Influence of Ostium combined with autologous platelet growth factors. *Biomaterial*, **3**, pp.126-132.
8. Khurshid Z., M.S. Zafar, S. Hussain, A. Fareed, S. Yousaf, and F. Sefat, (2020). Silver-substituted hydroxyapatite. *In Handbook of Ionic Substituted Hydroxyapatites (pp. 237-257). Woodhead Publishing.*
9. BS ISO 13779-2:(2000): Implants for surgery—hydroxyapatite— Part 2: coatings of hydroxyapatite. *London: British Standards Institution.*
10. Thian ES, Huang J, Best SM, Barber ZH, Brooks RA, Rushton N, et al. (2006);The response of osteoblasts to nanocrystalline silicon substituted hydroxyapatite thin films. *Biomaterials*. 27: 2692–8.
11. Chin M.Y., A. Sandham, J. De Vries, van der Mei, H.C. and H.J. Busscher, (2007).

Biofilm formation on surface characterized micro-implants for skeletal anchorage in orthodontics. *Biomaterials*, **28(11),** pp.2032-2040.
12. Damschroder L.J., D.C. Aron, R.E. Keith, S.R. Kirsh, J.A. Alexander and J.C. Lowery, (2009). Fostering implementation of health services research findings into practice: a consolidated framework for advancing implementation science. *Implementation science*, **4(1),** pp.1-15.
13. Clement J.L. & P.S. Jarrett, (1994). Antibacterial silver. *Metal - based drugs*, **1(5-6),** pp.467-482.
14. Martínez-Gutierrez F., EP. Thi, JM. Silverman, CC. de Oliveira, SL. Svensson, AV. Hoek, EM. Sánchez, NE. Reiner, EC. Gaynor, EL. Pryzdial and EM. Conway, (2012). Antibacterial activity, inflammatory response, coagulation and cytotoxicity effects of silver nanoparticles. Nanomedicine: Nanotechnology, *Biology and Medicine*, **8 (3)**, pp. 328-336.
15. Naylor P.T., Q.N. Myrvik and A. Gristina, (1990). Antibiotic resistance of biomaterial-adherent coagulase-negative and coagulase-positive staphylococci. *Clinical Orthopaedics and Related Research®*, **261**, pp.126-133.
16. Rodrigues and A. Lebugle, (1998). Influence of ethanol in the precipitation medium on the composition, structure and reactivity of tricalcium phosphate. *Colloids and Surfaces A: Physicochemical and Engineering Aspects*, **145(1-3),** pp.191-204.
17. Feng W., L. Mu-Sen, L. Yu-Peng and Q. Yong-Xin, (2005). A simple sol–gel technique for preparing hydroxyapatite nanopowders. *Materials Letters*, **59(8-9),** pp.916-919.
18. Liu D.M., T. Troczynski and W.J. Tseng, (2002). Aging effect on the phase evolution of water-based sol–gel hydroxyapatite. *Biomaterials*, **23(4),** pp.1227-1236.
19. Thieme C., M. Kracker, K. Thieme, C. Patzig, T. Höche and C. Rüssel., (2019). Core–shell structures with metallic silver as nucleation agent of low expansion phases in $BaO/SrO/ZnO/SiO_2$ glasses. *CrystEngComm*, **21(29),** pp.4373-4386.
20. S.D Stookey, (1949). Coloration of glass by gold, silver, and copper. *Journal of the American Ceramic Society*, **32(8),** pp.246-249.
21. de Groot K., (1983). Ceramics of calcium phosphate: preparation and properties (pp. 100-114). *CRC Press, Boca Raton, FL*.
22. Kamiya K., T. Yoko, K. Tanaka and Y. Fujiyama, (1989). Growth of fibrous hydroxyapatite in the gel system. *Journal of materials science*, **24(3),** pp.827-832. 32.
23. Wu J.M. & T.S. Yeh, (1988). Sintering of hydroxylapatite-zirconia composite materials. *Journal of materials science*, **23(10),** pp.3771-3777.
24. Zhou J., X. Zhang, J. Chen, S. Zeng and K. De Groot, (1993). High temperature characteristics of synthetic hydroxyapatite. *Journal of materials science: materials in medicine*, **4(1),** pp.83-85.5.
25. Berzina-Cimdina L. and N. Borodajenko, (2012). Research of Calcium Phosphates Using Fourier Transform Infrared Spectroscopy. *Infrared spectroscopy-materials science, engineering and technology*, 12(7), pp.251-263.
26. Raynaud S., E. Champion, D. Bernache-Assollant and P. Thomas, (2002). Calcium phosphate apatites with variable Ca/P atomic ratio I. Synthesis, characterisation and thermal stability of powders. *Biomaterials*, **23(4),** pp.1065-1072.
27. Hudon P. & I.H. Jung, (2015). Critical evaluation and thermodynamic optimization of the $CaO-P_2O_5$ system. *Metallurgical and Materials Transactions B*, **46(1),** pp.494-522.
28. Enderle R., F. Götz-Neunhoeffer, M. Göbbels, F.A. Müller and P. Greil, (2005). Influence of magnesium doping on the phase transformation temperature of β-TCP ceramics examined by Rietveld refinement. *Biomaterials*, **26(17),** pp.3379-3384.

29. Meejoo S., W. Maneeprakorn and P. Winotai, (2006). Phase and thermal stability of nanocrystalline hydroxyapatite prepared via microwave heating. *Thermochimica acta*, **447(1),** pp.115-120.
30. Destainville, E. Champion, D. Bernache-Assollant and E. Laborde, (2003). Synthesis, characterization and thermal behavior of apatitic tricalcium phosphate. *Materials Chemistry and Physics*, **80(1),** pp.269-277.
31. Zakeri M., M.R. Rahimipour and B. Jamal Abbasi, (2013). Mechanochemical synthesis of nanocrystalline hydroxyapatite via mechanical alloying. *Materials Technology*, **28(3),** pp.159-164.
32. Pleshko N., A. Boskey and R. Mendelsohn, (1991). Novel infrared spectroscopic method for the determination of crystallinity of hydroxyapatite minerals. *Biophysical journal*, **60(4),** pp.786-793.
33. Termine J.D. & A.S. Posner, (1966). Infra-red determination of the percentage of crystallinity in apatitic calcium phosphates. *Nature*, **211(5046),** pp.268-270.].
34. Shirkhanzadeh M., M. Azadegan, F.Q. Liu. (1995) Bioactive Delivery Systems for the Slow Release of Antibiotics: Incorporation of Ag^{+} Ions into Micro-Porous *Hydroxyapatite Coatings Materials Letters* **24** pp. 7 – 12. http:// dx.doi. org/10. 1016/ 0167 -577X(95)00059-3
35. Nath S., S. Kalmodia, B. Basu. Densification, (2010). Phase Stability and In Vitro Biocompatibility Property of Hydroxyapatite-10 w.t% Silver Composites. *Journal of Materials Science: Materials in Medicine* **21** pp. 1273 – 1287. http://dx.doi.org/10.1007/s10856-009-3939-2
36. Samani S., S.M. Hossainalipour, M. Tamizifar,H.R. Rezaie. In Vitro Antibacterial (2013)Evaluation of Sol–Gel Derived Zn-, Ag-, and (Zn + Ag)-Doped Hydroxyapatite Coatings Against Methicillin-Resistant Staphylococcus aureus *Journal of Biomedical Materials Research Part A* **101A**: pp. 222 – 230. http://dx.doi.org/10.1002/jbm.a.34322 24.
37. Li J.D., Y.B. Li, Y. Zuo, G.Y. Lv, W.H. Yang, Zh.Y. Tian. (2006) Antibacterial Effect and Security Evaluation on Nano-Hydroxyapatite Bearing Cu^{2+} and Zn^{2+} *Materials Science Forum* **510 – 511** pp. 890 – 893. 25.
38. Kolmas J., E. Groszyk, D. Kwiatkowska-Róhycka. (2014): Substituted Hydroxyapatites with Antibacterial Properties *BioMedical Research International* pp. 1 – 5.
39. Stanić V., D. Janaćković, S. Dimitrijević, S.B. Tanasković, M. Mitrić, M.S. Pavlović, A. Krstić, D. Jovanović and S. Raičević, (2011). Synthesis of antimicrobial monophase silver-doped hydroxyapatite nanopowders for bone tissue engineering. *Applied Surface Science*, **257 (9),** pp. 4510 - 4518.